J Mater Sci (2016) 51:8005–8017

Quantifying structural and electromagnetic interference (EMI) shielding properties of thermoplastic polyurethane–carbon nanofiber/magnetite nanocomposites

Zehra Durmus[1,*], Ali Durmus[2], M. Yunus Bektay[3], Huseyin Kavas[4], Ibrahim Saim Unver[5], and Bekir Aktas[5]

[1] *Department of Pharmaceutical Biotechnology, Faculty of Pharmacy, Bezmialem Vakıf University, Fatih, 34093 Istanbul, Turkey*
[2] *Department of Chemical Engineering, Faculty of Engineering, Istanbul University, Avcilar, 34320 Istanbul, Turkey*
[3] *Department of Pharmacology, Faculty of Pharmacy, Bezmialem Vakıf University, Fatih, 34093 Istanbul, Turkey*
[4] *Department of Engineering Physics, Istanbul Medeniyet University, Kadıköy, Istanbul, Turkey*
[5] *Department of Physics, Gebze Technical University, 41400 Kocaeli, Turkey*

Received: 31 March 2016
Accepted: 14 May 2016
Published online: 31 May 2016

ABSTRACT

In this study, mixed-structure carbon–magnetite nanocomposites were prepared by decorating of carbon nanofiber (CNF) surfaces with magnetite (Fe_3O_4) nanoparticles synthesized via reflux method and characterized. The compositions of CNF–Fe_3O_4 nanocomposites were varied using different amounts of CNF into the Fe_3O_4 synthesis medium as 25/75, 50/50, and 75/25 (w/w). These nanocomposites were then used as functional fillers to prepare flexible, thermoplastic polyurethane (TPU)-based electromagnetic interference (EMI) shielding composites by solution mixing method. Structural features of fillers, morphological, and electromagnetic properties of flexible composites were studied. It was found that the magnetite nanoparticles with the average size of 8–10 nm were formed and successfully covered the oxidized CNF surfaces. It was also found that the resulting CNF–Fe_3O_4 nanocomposites exhibited sufficiently high saturation magnetization (M_s) values compared to Fe_3O_4. These CNF–Fe_3O_4 nanocomposites were embedded into TPU phase by employing the weight percent of 20 wt%. The flexible TPU–CNF–Fe_3O_4 nanocomposite having the composition of 80–5–15 wt% showed the reflection loss (*RL*) value of −32 dB which signified that the composite material could absorb the 97 % of an incident electromagnetic wave at around 12.14 GHz.

Address correspondence to E-mail: zdurmus@bezmialem.edu.tr

DOI 10.1007/s10853-016-0069-3

Introduction

Shielding of electromagnetic radiation is one of the most challenging topics which have recently attracted great industrial and scientific interests in materials science due to its increasing importance in several applications such as communication systems, military, defense and aerospace engineering, and medical and electronics devices. Shielding of electromagnetic waves can be basically achieved either reflecting or absorbing of an incident wave and specifically required using of structurally designed materials and/or material combinations depending on the shielding effectiveness and mechanism needed. It is simply known that the conducting materials such as metal particles, sheets, and various forms of carbons and conductive polymers can be used to reflect the electromagnetic waves while different types of magnetic materials could be employed to absorb the electromagnetic waves. Soft and hard ferrites are the most extensively studied magnetic materials for the electromagnetic interference (EMI) shielding, specifically microwave or radar absorbing, applications [1–8]. The unique structural and physical features of single or mixed-structure ferrites make them proper materials for absorbing of electromagnetic waves in the relatively high-frequency region (8–18 GHz) which is an important range for radar absorbing and military applications. In recent years, combination of magnetic materials with both various forms of carbon materials such as carbon fiber, carbon nanotubes (CNTs), graphite and graphene derivatives, and carbon nanofiber (CNF) and also with different polymers by regarding the composite approaches have been studied to improve the shielding efficiency (SE) and extend the processability and applications of such materials [9–14]. Furthermore, a few studies have also been reported on the electromagnetic properties of polymer composites including of carbon/ferrite fillers as functional filler and conductive polymers as matrix [15, 16].

CNF is a one-dimensional (1D), more versatile, low-cost, and commercially available form of carbon materials compared to carbon nanotubes. CNF and modified CNFs have been used in various applications such as manufacturing of biomedical devices, filters, drug delivery systems, energy storage devices, and sensors. [17–20]. Decoration of CNFs with various types of nanoparticles leads to prepare novel and structurally designed multi-component functional nanocomposites. Fibrous structure of CNF might also prevent the self-agglomeration of nanoparticles and provide them a template to form a 1D alignment. In case of magnetic nanoparticles, CNF leads to prepare multi-layered "magnetic-conductive-magnetic" structure besides the 1D alignment of magnetic nanoparticles, and therefore the electromagnetic properties of resulted structure could be different from the bulk form of magnetic component. To the best of our knowledge, only a few studies have yet been reported on the characterization of electromagnetic properties and EMI shielding performances of CNF-magnetic nanoparticle composites. Mutlu et al. studied on the EMI shielding effectiveness of multifunctional Fe_3O_4/CNF composites in the X-band region (8.2–12.4 GHz) [21]. They prepared the Fe_3O_4/CNF composites by dispersing of surface-modified magnetite nanoparticles into poly(acrylonitrile) (PAN) solution and carbonization of electrospun PAN fibers. They examined the effects of various parameters such as Fe_3O_4 content, carbonization temperature, and sample thickness on total shielding efficiency (SE_{total}) of different samples. They found that the composite of 5 wt% Fe_3O_4 with the thickness of 0.7 mm exhibited maximum EMI shielding efficiency (67.9 dB) and the absorption was the dominant factor for shielding. Panels et al. used a similar methodology, carbonization of PAN solution containing the iron oxide precursor, iron (III) acetylacetonate, to prepare electrically conducting and magnetically active CNF mats with hierarchical pore structures [22]. On the other hand, it is a well-known fact that the electromagnetic properties and related EMI shielding performances of magnetite and/or other ferrite nanoparticles depend on the structural and physical features of these materials such as the particle size, chemical composition, crystal structure, and crystallite size. [23–28]. Liu et al. investigated the effect of granular size of Fe_3O_4 particles within the range of 20–250 nm on the high-frequency dynamic magnetic properties, the complex permeability, and permittivity and reflection loss (*RL*) values, of particles in a frequency range of 1–15 GHz [29]. They reported that the particles with the sizes of 20 and 100 nm showed better absorption performance than that of bigger sizes at the frequencies under 15 GHz. They also concluded that the Fe_3O_4 nanoparticles having the average size under 100 nm exhibited satisfying performance in microwave attenuation and could be considered as potential candidate for

microwave absorption applications. It could be expected that the variation in the electromagnetic properties of magnetic nanoparticles with the average size of particles is mainly related to the ratio of surface and bulk atoms. It is known that the size reduction in the magnetic nanoparticles yields higher surface/volume ratio which leads to different properties than the bulk materials. Decreasing in the particle size results in reducing in the number of spins cooperatively linked within the particle and surface effects becomes much more important on the magnetic properties of particles. Number of surface atoms in magnetic nanoparticles can be alternatively increased by forming lateral (1D or 2D) clustering.

In this study, chemically oxidized CNFs were decorated with the magnetite (Fe_3O_4) nanoparticles synthesized via reflux/co-precipitation method. Structural and electromagnetic properties of CNF–Fe_3O_4 nanocomposites were characterized. These nanocomposites were also dispersed into thermoplastic polyurethane (TPU) phase to prepare flexible EMI shielding composites. EMI shielding performances of TPU–CNF–Fe_3O_4 composites within the X-band were quantified depending on the sample composition.

Experimental

Materials

Iron (III) chloride hexahydrate, ($FeCl_3.9H_2O$), iron (II) tetrahydrate ($FeCl_2.4H_2O$) ammonia solution (NH_3), sulfuric acid (H_2SO_4 98 % fuming), nitric acid (HNO_3), and tetrahydrofuran (THF) were purchased from Sigma-Aldrich. All the chemicals employed in the study were analytical grade and used as-received without a purification.CNF was a commercial grade material, Pyrograf®-III (PR-24-XT-LHT). TPU, used as polymer matrix in the study, was also a commercial grade polyester-based polyurethane (Desmopan® 3380A, shore hardness: 80A, *d*: 1.16 g cm^{-3}), kindly donated by Bayer (Turkey).

Oxidation of CNF

Oxidation of CNFs was performed according to the previously reported method [30]. In this method, approximately 1 g of CNF powder was dispersed into a 250 ml of concentrated H_2SO_4 and HNO_3 mixture (3:1, v/v) then the suspension was sonicated for 2 h. This suspension was transferred into a 500 ml flask equipped with a condenser and refluxed at 90 °C for 10 h by stirring vigorously. The mixture was cooled to room temperature and filtered. The filtrate was washed several times with excess of deionized water until no residual acid was present (pH >6). The filtrate, oxidized CNF, was then dried in a vacuum oven at 70 °C for 6 h.

Synthesis of CNF–Fe_3O_4 nanocomposites

CNF–Fe_3O_4 nanocomposites were prepared by the synthesis of magnetite nanoparticles via reflux/co-precipitation method in the reaction medium containing of various amounts of oxidized CNF. A certain amount of oxidized CNF powder was introduced into an aqueous solution of ferrite salts, having the Fe(III):Fe(II) molar ratio of 2:1, and mechanically mixed at 40 °C for 15 min. Then the pH value of suspension was adjusted to 11 using a proper amount of ammonia solution. This suspension was then refluxed at 90 °C for 6 h by continuously stirring under an inert atmosphere by using argon gas with the flow rate of 100 ml/min. After the formation of magnetite nanoparticles, CNF-Fe_3O_4 nanocomposite powders were separated from the aqueous solution by a simple filtration and washed with distilled water several times then dried in a vacuum oven at 80 °C, overnight. The composition of CNF–Fe_3O_4 composites were varied as 25/75, 50/50, and 75/25 (w/w) and the resulting samples were denoted as CNF-25, CNF-50, and CNF-75, respectively. The CNF-50 samples was also prepared according to the same procedure using the pristine (un-oxidized) CNF for structural comparing to the oxidized counterpart.

Preparation of TPU–CNF–Fe_3O_4 nanocomposites

The TPU–CNF–Fe_3O_4 composites were prepared via solution mixing method by dispersing of CNF–Fe_3O_4 powders into a 10 wt% of TPU solution. TPU was dissolved into THF and the CNF–Fe_3O_4 powder was suspended into the same solvent under the sonication for 15 min. The TPU solution was gradually introduced into the CNF–Fe_3O_4 suspension by vigorously stirring for 30 min. This mixture was also sonicated for 15 min then poured into Teflon petri dishes, dried

to constant weight and subsequently under vacuum at 50 °C for 24 h to ensure for removing of all solvent. Sample composition and notations are given in Table 1. The TPU/filler ratio was kept as 80/20 (w/w) for all samples but the amounts of CNF and Fe_3O_4 were varied as listed in Table 1.

Structural and physical characterization of samples

The microstructural features and morphological properties of CNF, Fe_3O_4, and CNF–Fe_3O_4 powders and TPU–CNF–Fe_3O_4 nanocomposites were characterized using of Fourier-Transform infrared spectroscopy (FTIR), X-ray diffraction (XRD), scanning electron microscopy (SEM), transmission electron microscopy (TEM), and atomic force microscopy (AFM) methods.

FTIR spectra of samples were recorded in transmission mode with a Bruker Alpha infrared spectrometer using the attenuated total reflectance (ATR) mode and germanium crystal, in the range of 400–4000 cm^{-1} with the resolution of 2 cm^{-1}. The XRD patterns of samples were obtained using a Rigaku Smart Lab XRD with Cu K_α radiation at room temperature. The morphological features of samples were investigated by a field emission SEM (FE-SEM, FEI Quanta FEG 450) and TEM (FEI Tecnai G2 Sphera) microscopes. In the SEM analysis, powder samples were directly imaged in the instrument after a proper sample preparation route, sputter-coated with gold. In the TEM analysis, a drop of diluted sample suspension in alcohol was dripped onto a TEM grid then dried and imaged in the instrument. Surface topography and height profiles of samples were examined by an atomic force microscopy (AFM, Park Systems XE 100E model) in non-contact mode. The AFM sample was prepared by drop-casting of a diluted suspension of nanocomposite onto a SiO_2 wafer. The droplet was then spread over the substrate using a spin coater (MTI VCT 100A).

Magnetic properties of samples were characterized with a VSM (LDJ Electronics Inc., Model 9600) at room temperature, in an applied field of 15 kOe. Electromagnetic shielding properties of TPU-CNF-Fe_3O_4 nanocomposites were determined according to the rectangular wave-guide technique using a vector network analyzer (VNA, HP 8510C) within the frequency range of 8–12 GHz. Nanocomposites samples were molded in a hot pres (under the conditions of 140 °C, 2 tons, for 3 min) as a rectangular sheets, with the dimensions of 10.2 × 22.8 mm in length and width, respectively, and having the thicknesses between 0.25 and 3.0 mm, for the microwave-absorbing measurements. The scattering parameters of samples for the reflection (S11 or S22) and absorption (S12 or S21) were determined. Full two-port calibration was performed to remove possible errors due to the directivity, source match, load match, etc., in both forward and reverse directions.

Results and discussion

Structural and morphological characterization of samples

Figure 1 shows the FTIR spectra of oxidized CNF, Fe_3O_4, and CNF–Fe_3O_4 nanocomposites. In this figure, the FTIR spectrum of oxidized CNF powder was denoted as *Ox*-CNF to identify the structural features of this material depending on the chemical modification route but it should be noted that the CNF–Fe_3O_4 nanocomposites were also prepared using the oxidized CNF. The oxidized CNF and CNF–Fe_3O_4 nanocomposites exhibited various peaks originated from the presence of different types of oxygen species onto the fiber surfaces due to the oxidation process. It can be clearly seen that the oxidized CNF showed a

Table 1 Compositions of polymer composites

Samples	Compositions (wt%)				Amounts of fillers (wt%)	
	TPU	CNF-25	CNF-50	CNF-75	CNF	Fe_3O_4
TPU–CNF	80				20	
TPU–Fe_3O_4	80					20
TPU–CNF-25	80	20			5	15
TPU–CNF-50	80		20		10	10
TPU–CNF-75	80			20	15	5

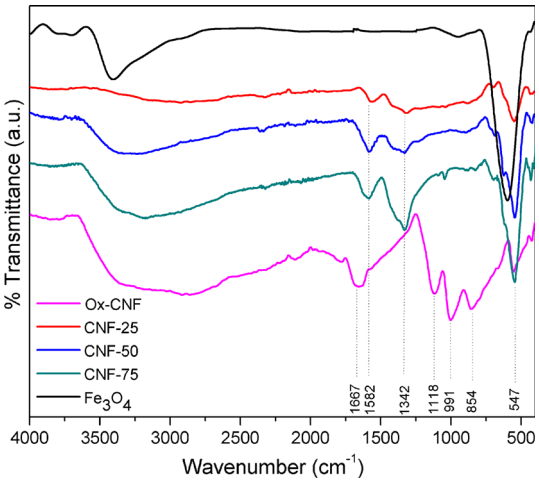

Figure 1 FTIR spectra of oxidized CNF, Fe_3O_4, and nanocomposite fillers.

very broad peak in the wavenumber range of 2500–3500 cm^{-1} which could be attributed to stretching of –OH groups due to the hydrophilic nature of oxidized surfaces. The intense peak observed in the FTIR spectrum of Fe_3O_4 at 3400 cm^{-1} also corresponds to stretching vibration of –OH groups. Peaks observed in the FTIR spectra of CNF-Fe_3O_4 samples at 1667 and 1582 cm^{-1} belong to the stretching vibration of C=O and the skeletal vibration of un-oxidized graphitic domains (aromatic C=C), respectively. Furthermore, the characteristic peaks observed at the wavenumbers of 1342, 1118, 991, and 854 cm^{-1} correspond to the stretching of C–O, asymmetric, and symmetric stretching of carbonyl groups $-CO_2$ and bending of C–O bonds, respectively. The characteristic vibration of inorganic lattice appears in the wavenumber range of 400–700 cm^{-1} for the Fe_3O_4 and CNF-Fe_3O_4 samples. Prepared CNF-Fe_3O_4 powders exhibited the following characteristic peaks of magnetite structure; (i) v_1 metal–oxygen band observed at 547 cm^{-1} which corresponds to intrinsic stretching vibration of metal at tetrahedral site ($Fe_{tetra} \leftrightarrow O$) and (ii) v_2 metal–oxygen band observed at 445 cm^{-1} which assigned to stretching vibration of metal at octahedral site ($Fe_{octa} \leftrightarrow O$).

XRD patterns of pristine CNF and oxidized CNF and CNF–Fe_3O_4 nanocomposites are given in Fig. 2a, b, respectively. As seen in Fig. 2a, pristine CNF and oxidized CNF showed characteristic diffraction peaks at about $2\theta = 26^{\circ}$ and 43° which correspond to the (002) and (101) planes of graphitic arrangement in the

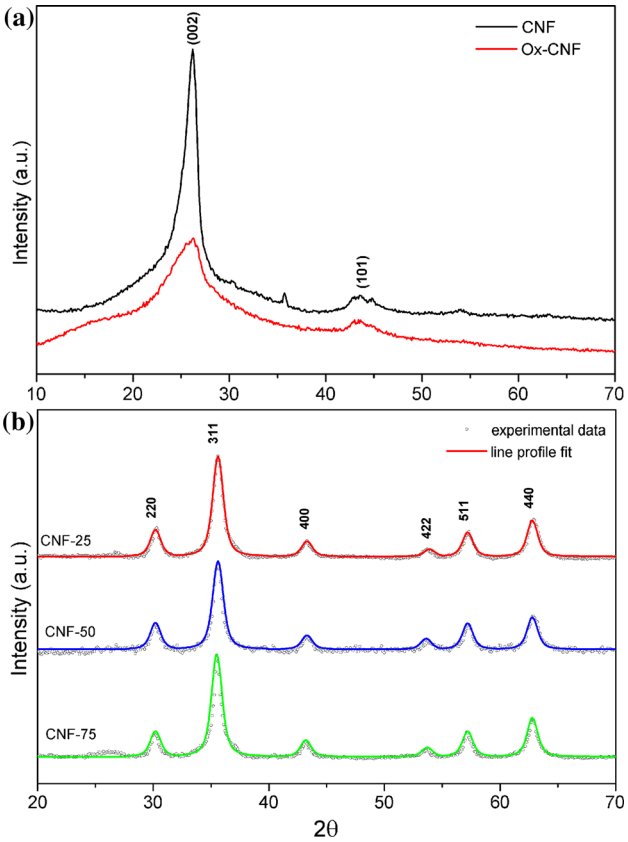

Figure 2 XRD patterns of **a** pristine and oxidized CNF and **b** nanocomposite fillers.

CNF walls, respectively. But, it was found that the chemical oxidation yielded to decrease the peak intensity because the formation of oxidized species onto CNF surface possibly deteriorated the surface character and crystalline arrangement of CNF, as expected. The XRD patterns of CNF–Fe_3O_4 samples indicated that the magnetite structure was successfully formed in the reaction medium including various amount of oxidized CNF. All diffraction peaks were indexed by the cubic structure of Fe_3O_4 (JCPDS no. 19-629). As seen in Fig. 2b, characteristic diffraction peaks of Fe_3O_4 structure characterized with the miller indices of (220), (311), (400), (422), (511), (440), (026), and (335) are quite broad which implies the formation of very small crystallite size according to the Scherer equation. The average crystallite size of magnetite nanoparticles was estimated using the line profile fitting method [31]. The line profile fitting curves of CNF-Fe_3O_4 samples are labeled as solid lines in Fig. 2b. The average crystallite size of magnetite nano particles (D) was determined to be

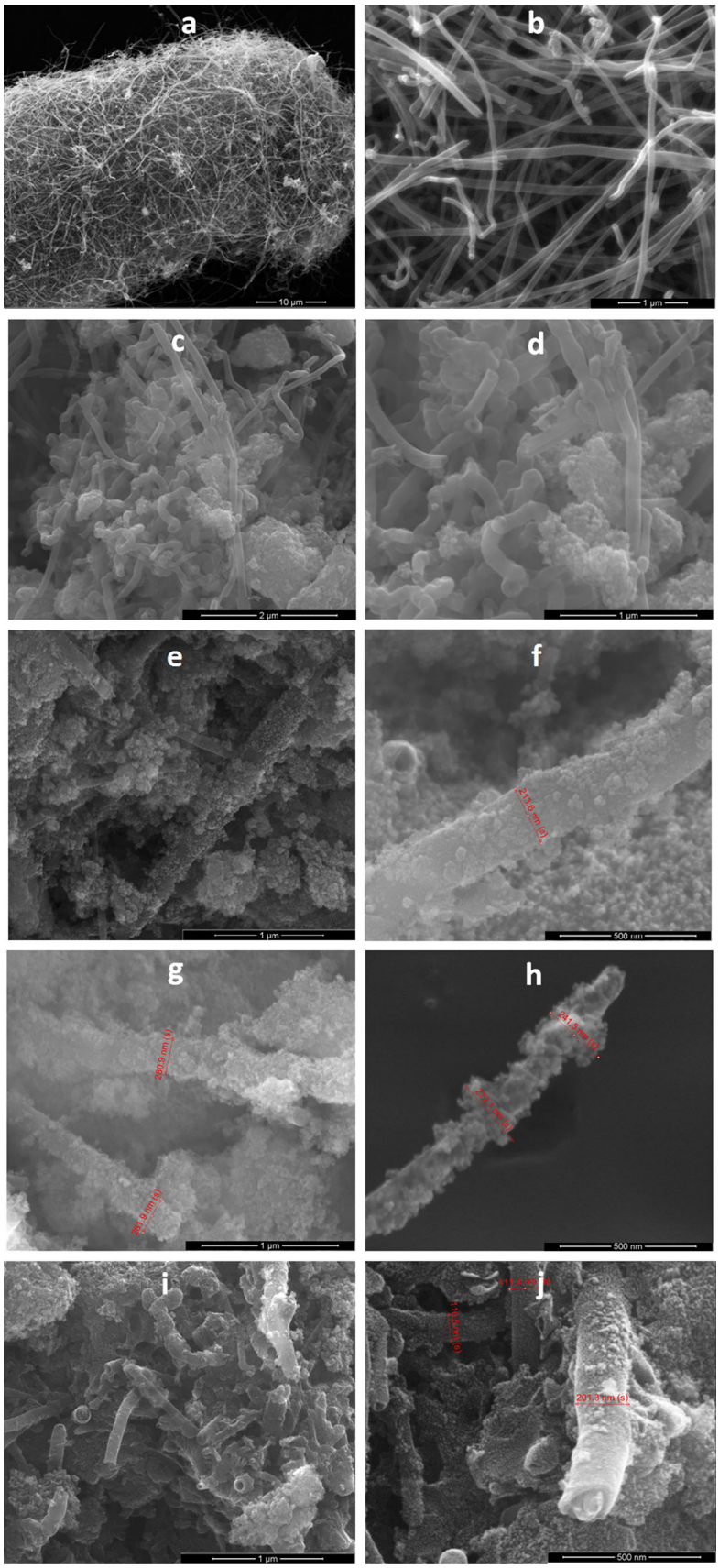

Figure 3 SEM micrographs of pristine CNF (**a**, **b**), CNF-50 prepared with pristine CNF (**c**, **d**) and CNF-25 (**e**, **f**), CNF-50 (**g**, **h**) and CNF-75 (**i**, **j**) samples prepared with oxidized CNF.

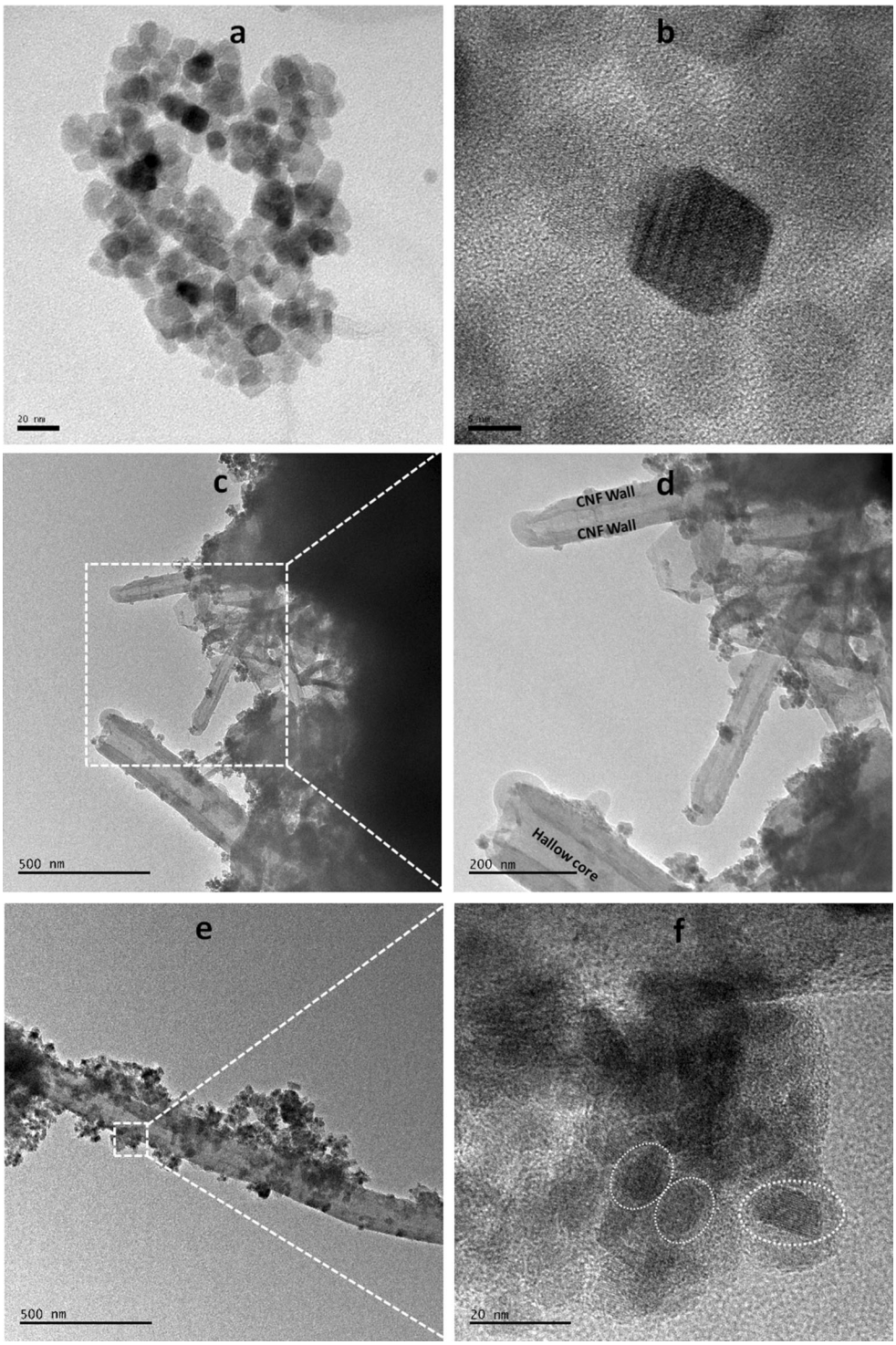

Figure 4 TEM micrographs of Fe_3O_4 (**a**, **b**) and CNF-50 samples (**c–f**) at different magnifications.

8 ± 3 nm by line profile fitting for the CNF-Fe_3O_4 nanocomposites independent from the composition.

SEM micrographs of pristine CNF and CNF-Fe_3O_4 nanocomposites are given in Fig. 3. As seen in Fig. 3a, the bundle form of CNF is a large particle. Average size of a cocoon-like bundle of as 35–60 μm. Figure 3b demonstrates the transparency of CNF structure at a higher magnification. Average fiber

diameter was about 120 nm. Figure 2c, d illustrates the microstructure of control sample, CNF-50, prepared using the pristine CNF. It is clearly seen that there is no interaction between the components, and this sample is more likely a physical mixture of CNFs and Fe_3O_4 nanoparticles. Very large magnetite agglomerates can also be seen in these images. But, it should also be noticed that the CNFs given in Fig. 2c, d are highly disentangled possibly due to the sonication. The SEM images of CNF-25, CNF-50, and CNF-75 samples obviously signified that the oxidized CNF surfaces were successfully decorated with the magnetite nanoparticles. The average diameter of "Fe_3O_4 decorated CNF" was estimated approximately 215 ± 42 nm while that of pristine CNF was about 120 nm. This increase in the diameter of modified CNF implied that the oxidized CNFs were covered with Fe_3O_4 agglomerates. In these figures, particularly in Fig. 3h, it can be clearly seen that there is no uncovered domains onto the oxidized CNF surfaces with the magnetite nanoparticles agglomerates. But, the increasing amount of CNF into the nanocomposite composition yielded both the formation of uncovered domains onto fiber surfaces and some large magnetite aggregates as seen in Fig. 3i, j.

Figure 4 shows TEM micrographs of magnetite nanoparticles and CNF-50 samples at different magnifications. The TEM images of magnetite indicated that the well-crystallized Fe_3O_4 nanoparticles having a very narrow size distribution were obtained. The average particle size can be estimated in the range of 10–15 nm.

Figure 5 illustrates the AFM topography image, line profile, and line histogram of CNF-50 nanocomposite prepared with the oxidized CNF. Agglomerated nanofibers consisting of randomly aligned fibers covered well with the magnetite nanoparticles can be seen in the AFM topography image given in Fig. 5b,

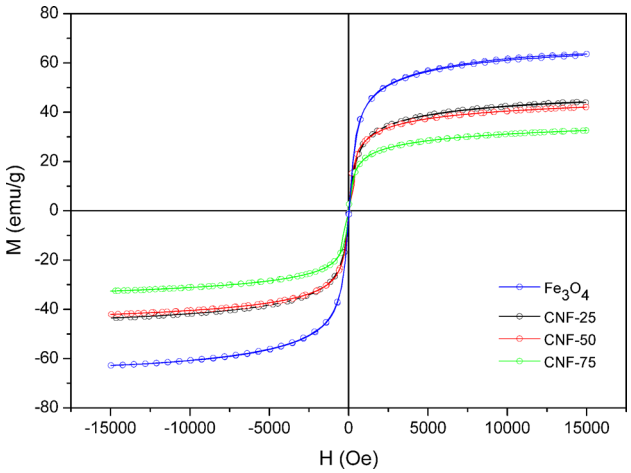

Figure 6 Magnetic hysteresis loops of Fe_3O_4 and CNF–Fe_3O_4 nanocomposite fillers recorded at room temperature.

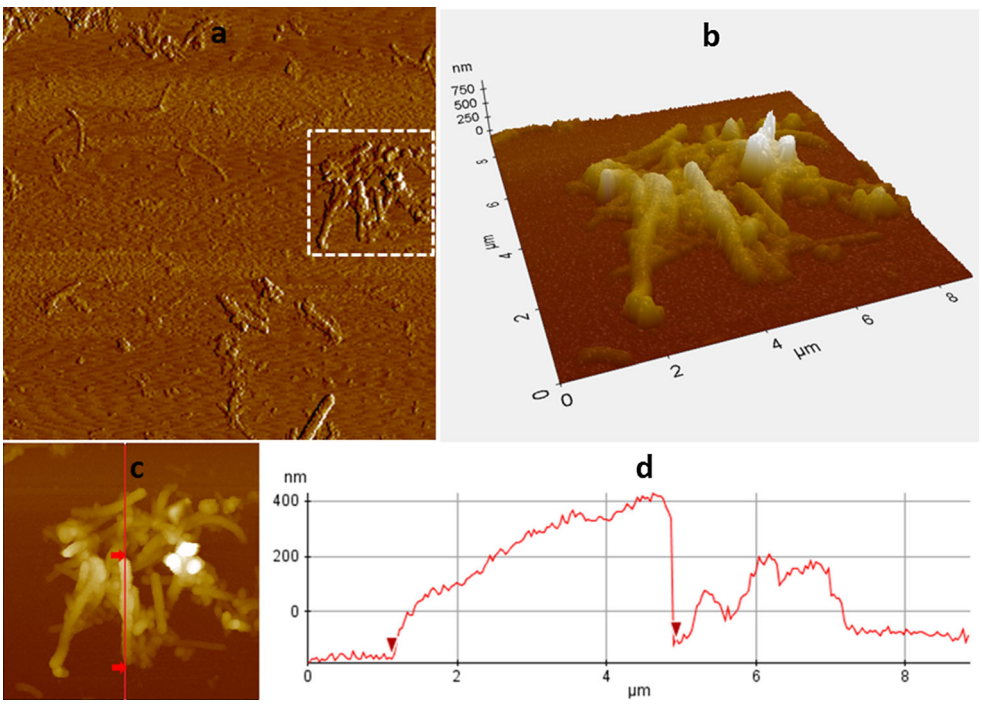

Figure 5 AFM topography image, line profile, and line histogram of CNF-50 nanocomposite.

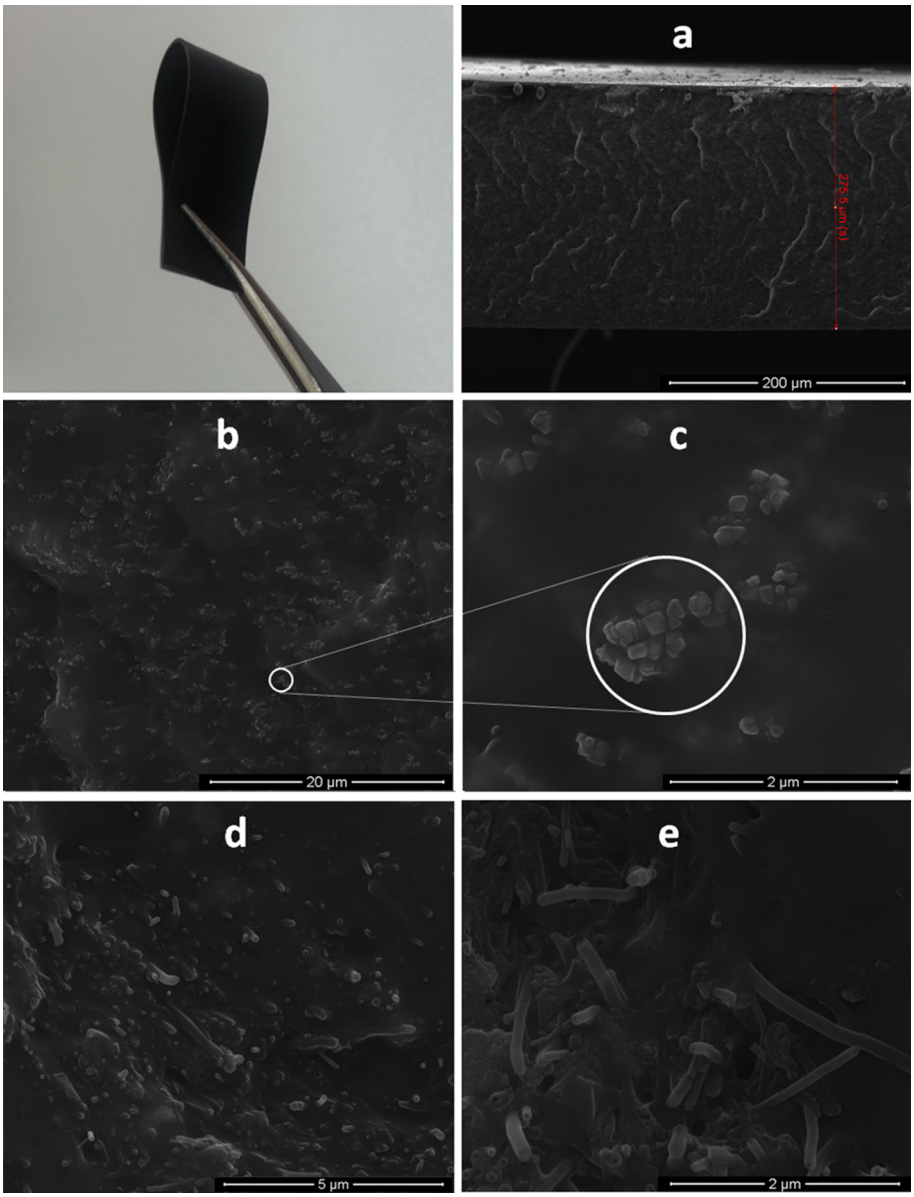

Figure 7 Photograph and **a–c** SEM micrographs of TPU–Fe_3O_4 film, **d** TPU–CNF-50 prepared with oxidized CNF and **e** TPU–CNF-50 prepared with pristine CNF.

c. An average fiber length was estimated about 4–6 µm by examining the 3D profile and line histogram of sample image given in Fig. 5b, d, respectively. This fiber length is possibly shorter than those of the pristine CNF. It might be concluded that the chemical treatment with strong acids and long-time sonication could break down the fibers and yielded lower aspect ratio values. Aspect ratio (A_f) can be defined as the ratio of length (L) to thickness (h) or diameter (d) for 1D and 2D materials. The A_f value is considered as one of the critical parameters for such kind of fillers improving the physical (mainly rheological and mechanical) properties of composite materials. Based on the average length (4–6 µm by AFM images) and thickness (215 nm by SEM images) values of CNF-50 sample, the A_f value of functional nanocomposites could be estimated as in the range of 20–30.

It is a well-known fact that the VSM analysis is a typical characterization method for magnetic properties of a material. Figure 6 compares the magnetic hysteresis loops of CNF–Fe_3O_4 nanocomposites to that of magnetite. It can be clearly seen that the saturation magnetization (M_s) values of functional fillers

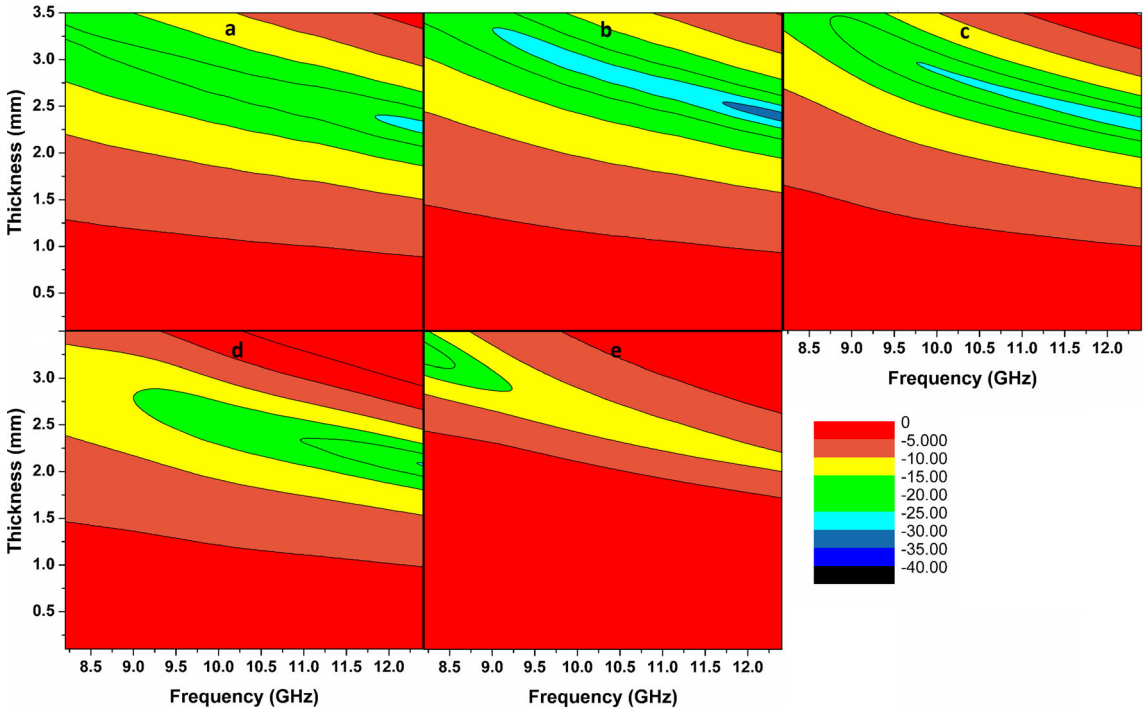

Figure 8 Dependence of *RL* value of **a** TPU–Fe_3O_4, **b** TPU–CNF-25 **c** TPU–CNF-50, **d** TPU–CNF-75, and **e** TPU–CNF samples on the sample thickness and frequency.

decreased with the increasing amount of CNF into the composition, as expected. But, it could be concluded that all mixed-structure fillers showed fairly enough magnetism as seen in figure inset. The inset photograph shows the response of CNF-50 powders dispersed into aqueous medium to an external magnetic field.

Figure 7 demonstrates the SEM micrographs of TPU-Fe_3O_4 films and TPU–CNF-50 samples at different magnifications. The first photograph shows the flexibility of TPU–Fe_3O_4 composite. It was found that the small agglomerates of Fe_3O_4 nanoparticles were homogenously dispersed into the TPU matrix as seen in Fig. 7a-c. SEM images of TPU–CNF-50 composites prepared with the oxidized and pristine CNFs are given in Fig. 7d, e, respectively. It can be noticed in Fig. 7d that the fibers of CNF-50 nanocomposite prepared with the oxidized CNF were embedded well into the TPU matrix and the filler-polymer interactions were much better than the counterpart nanocomposite prepared with the pristine CNF. This result clearly indicated that both issues; (i) oxidation of CNFs and (ii) decoration with the magnetite nanoparticles lead to increase the dispersion homogeneity of multi-structured fillers into the TPU matrix in point of view composite science.

The *RL* values of samples were calculated with the universal formula defined below and using the electromagnetic parameters of samples depending on the frequency.

$$RL(\mathrm{dB}) = 20\log\left|\frac{Z_{\mathrm{in}}-1}{Z_{\mathrm{in}}+1}\right|, \tag{1}$$

$$Z_{\mathrm{in}} = \sqrt{\frac{\mu_r}{\varepsilon_r}}\tanh\left(j\frac{2\pi df}{c}\sqrt{\mu_r\varepsilon_r}\right), \tag{2}$$

where Z_{in} is the input impedance, ε_r is the complex dielectric permittivity, and μ_r is the complex magnetic permeability of sample with a constant thickness (d) at a given frequency (f). The complex dielectric permittivity ($\mu_r = \mu' - j\mu''$) and magnetic permeability ($\mu_r = \mu'\text{-}j\mu''$) values of samples were measured by rectangular wave-guide method in the frequency range of 8–12 GHz, but the curves of real and imaginary parts of such parameters were not given here.

Figure 8 shows the contour plots of *RL* dependence of TPU–CNF-Fe_3O_4 composites as a function of sample thickness and frequency. It was found that the matching thickness band (the *RL* below −15 dB) reduced with the increasing of frequency. It can also be seen that this band is relatively broad for the TPU–

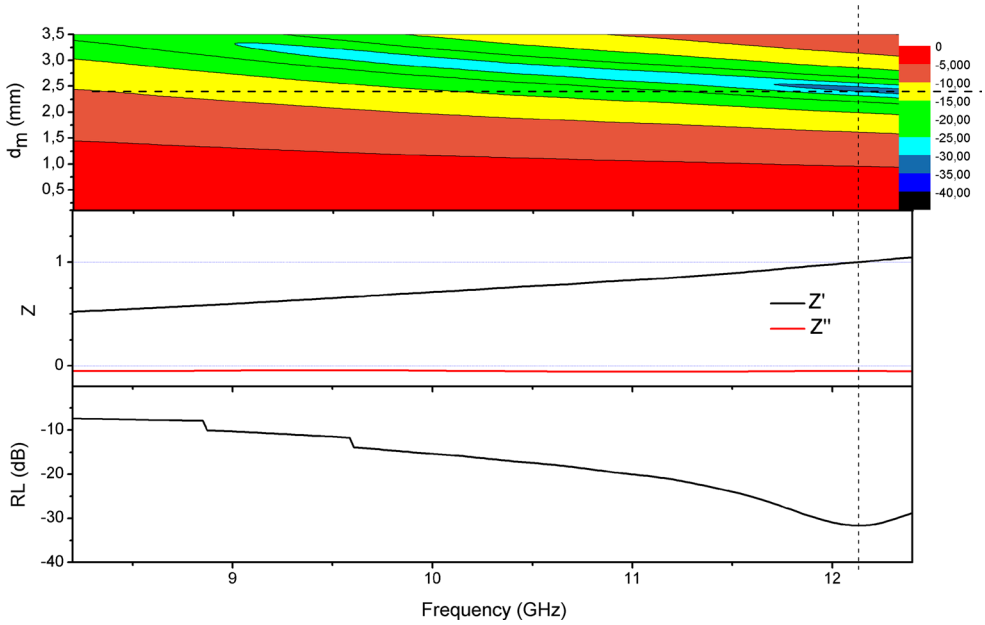

Figure 9 The *RL* surface plot as a function of matching thickness and frequency, complex matching impedance, and *RL* curves as a function of frequency for the TPU–CNF-25 sample.

CNF-25 sample but then it becomes narrow with the increasing amount of CNF into the samples composition. It was also found that the TPU–CNF-25 sample yielded minimum *RL* values marked as a dark blue band in the high-frequency region.

Figure 9 illustrates the *RL* surface plot as a function of matching thickness and frequency, complex matching impedance, and *RL* curves as a function of frequency for the TPU–CNF-25 sample. The *RL* curve of sample exhibits a distinctive peak at 12.14 GHz having the *RL* value of −32 dB. The *RL* values below −20 dB for a sample signifies that this material is a promising candidate as electromagnetic wave absorbing material because it can absorb 90 % of the wave. In this study, it was found the TPU–CNF-25 sample can absorb 97 % of an incident wave in X-band therefore it can be considered as a promising material for radar absorbing applications.

Conclusion

In this study, various compositions of CNF–Fe_3O_4 nanocomposites were prepared by successfully decorating of oxidized CNFs with the magnetite nanoparticles synthesized via reflux/co-precipitation method. These materials were then dispersed into TPU matrix to prepare flexible EMI shielding polymer composites. Structural features, electromagnetic properties, and EMI shielding performances of TPU–CNF–Fe_3O_4 composites were quantified depending on the sample composition and thickness. It was found that the presence of oxidized CNFs in the synthesis medium of Fe_3O_4 induced the formation of one-dimensionally aligned magnetite nanoparticles and substantially prevent the formation of large magnetite agglomerates. Moreover, introducing of CNFs into a multi-component composite formulation lead to form layered structure and could yield a higher EMI shielding performance than composites prepared with a single filler. It was found that the TPU–CNF-25 sample (having the composition of 80TPU/5CNF/15Fe_3O_4 wt% and the thickness about 2.5 mm) showed a *RL* value of −32 dB at 12.14 GHz. Consequently, it can be concluded that the resulting, highly flexible TPU/CNF/Fe_3O_4 composites can be used in various EMI shielding applications in the X-band.

Acknowledgements

This study was supported by TUBITAK, The Scientific and Technological Research Council of Turkey, with the Project Number of 213M462.

References

[1] Abbas SM, Chandra M, Verma A, Chatterjee R, Goel TC (2006) Complex permittivity and microwave absorption properties of a composite dielectric absorber. Composites A 37:2148–2154

[2] Das S, Nayak GC, Sahu SK, Routray PC, Roy AK, Baskey H (2015) Microwave absorption properties of double-layer composites using CoZn/NiZn/MnZn-ferrite and titanium dioxide. J Magnet Magnet Mater 377:111–116

[3] Heo J., Choi D., Hong J., Layer-by-Layer self-assembled ferrite multilayer nanofilms for microwave absorption, J Nanomater. (2015) Article ID 164619

[4] Tyagi S, Baskey HB, Agarwala RC, Agarwala V, Shami TC (2011) Development of hard/soft ferrite nanocomposite for enhanced microwave absorption. Ceram Int 37:2631–2641

[5] Della Pina C, Falletta E, Ferretti AM, Ponti A, Gentili GG, Verri V, Nesti R (2015) Microwave characterization of magnetically hard and soft ferrite nanoparticles in K-band. J Appl Phys 116:154306

[6] Jacobo SE, Bercoff PG, Herme CA, Vives LA (2015) Sr hexaferrite/Ni ferrite nanocomposites: magnetic behavior and microwave absorbing properties in the X-band. Mater Chem Phys 157:124–129

[7] Ghodake JS, Kambale RC, Shinde TJ, Maskar PK, Suryavanshi SS (2016) Magnetic and microwave absorbing properties of Co^{2+} substituted nickel-zinc ferrites with the emphasis on initial permeability studies. J Magnet Magnet Mater 401:938–942

[8] Gama AM, Rezende MC (2013) Complex permeability and permittivity variation of radar absorbing materials based on MnZn ferrite in microwave frequencies. Mater Res 16:997–1001

[9] Durmus Z, Durmus A, Kavas H (2015) Synthesis and characterization of structural and magnetic properties of graphene/hard ferrite nanocomposites as microwave-absorbing material. J Mater Sci 50:1201–1213. doi:10.1007/s10853-014-8676-3

[10] Durmus Z, Kavas H, Durmus A, Aktas B (2015) Synthesis and micro-structural characterization of graphene/strontium hexaferrite ($SrFe_{12}O_{19}$) nanocomposites. Mater Chem Phys 163:439–445

[11] Verma M, Singh AP, Sambyal P, Singh BP, Dhawan SK, Choudhary V (2015) Barium ferrite decorated reduced graphene oxide nanocomposite for effective electromagnetic interference shielding. Chem Phys Phys Chem 17:1610–1618

[12] Zhang Q, Zhu M, Zhang Q, Li Y, Wang H (2009) The formation of magnetite nanoparticles on the sidewalls of multi-walled carbon nanotubes. Comp Sci Tech 69:633–638

[13] Zhang T, Huang D, Yang Y, Kanga F, Gub J (2013) Fe_3O_4/carbon composite nanofiber absorber with enhanced microwave absorption performance. Mater Sci Eng B 178:1–9

[14] Chen D, Quan H, Huang Z, Luo S, Luo X, Deng F (2014) Electromagnetic and microwave absorbing properties of RGO@hematite core-shell nanostructure/PVDF composites. Comp Sci Tech 102:126–131

[15] Yang R-B, Reddy PM, Chang C-J, Chen P-A, Chen J-K, Chang C-C (2016) Synthesis and characterization of Fe_3O_4/polypyrrole/carbon nanotube composites with tunable microwave absorption properties: role of carbon nanotube and polypyrrole content. Chem Eng J 285:497–507

[16] Luo J, Xu Y, Yao W, Jiang C, Xu J (2015) Synthesis and microwave absorption properties of reduced graphene oxide-magnetic porous nanospheres-polyaniline composites. Comp Sci Tech 117:315–321

[17] Stout DA (2015) Recent advancements in carbon nanofiber and carbon nanotube applications in drug delivery and tissue engineering. Current Pharm Design 21:2037–2044

[18] Adabi M, Saber R, Naghibzadeh M, Faridbod F, Faridi-Majidi R (2015) Parameters affecting carbon nanofiber electrodes for measurement of cathodic current in electrochemical sensors: an investigation using artificial neural network. RSC Adv 5:81243–81252

[19] Wang CJ, Chen TC, Lin J-H, Huang PR, Tsai HJ, Chen CS (2015) One-step preparation of hydrophilic carbon nanofiber containing magnetic Ni nanoparticles materials and their application in drug delivery. J Colloid Inter Sci 440:179–188

[20] Song MJ, Kim T, Kim YB, Shin MW (2015) Self-standing, binder-free electrospun Co_3O_4/carbon nanofiber composites for non-aqueous Li-air batteries. Electrochim Acta 182:289–296

[21] Bayat M, Yang H, Ko FK, Michelson D, Mei A (2014) Electromagnetic interference shielding effectiveness of hybrid multifunctional Fe_3O_4/carbon nanofiber composite. Polymer 55:936–943

[22] Panels JE, Lee J, Park KY, Kang SY, Marquez M, Wiesner U, Joo YL (2008) Synthesis and characterization of magnetically active carbon nanofiber/iron oxide composites with hierarchical pore structures. Nanotechnology 19:455612

[23] Pardavi-Horvath M (2000) Microwave applications of soft ferrites. J Magn Magn Mater 215–216:171–183

[24] Özgür Ü, Alivov Y, Morkoç H (2009) Microwave ferrites, Part 1: fundamental properties. J Mater Sci-Mater Electron 20:789–834

[25] Peddis D, Cannas C, Musinu A, Ardu A, Orru F, Fiorani D, Lauretti S, Rinaldi D, Muscas G, Concas G, Piccaluga G (2013) Beyond the effect of particle size: influence of $CoFe_2O_4$ nanoparticle arrangements on magnetic properties. Chem Mater 25:2005–2013

[26] Deraz NM (2010) Size and crystallinity-dependent magnetic properties of copper ferrite nano-particles. J Alloys Compd 501:317–325

[27] Chia CH, Zakaria S, Yusoff M, Goh SC, Haw CY, Ahmadi Sh, Huang NM, Lim HN (2010) Size and crystallinity-dependent magnetic properties of $CoFe_2O_4$ nanocrystals. Ceramic Int 36:605–609

[28] Raghavender AT, Zadro K, Pajic D, Skoko Z, Biliskov N (2010) Effect of grain size on the neel temperature of nanocrystalline nickel ferrite. Mater Let 64:1144–1146

[29] Liu J, Zeng M, Yu R, Liu X, Zhu M (2014) Size influence to the high-frequency properties of granular magnetite nanoparticles. IEEE Trans Magn 50:2801304

[30] Choudhury A, Kar P (2011) Doping effect of carboxylic acid group functionalized multi-walled carbon nanotube on polyaniline. Composites B 42:1641–1647

[31] Wejrzanowski T, Pielaszek R, Opalinska A, Matysiak H, Lojkowski W, Kurzydlowski KJ (2006) Quantitative methods for nanopowders characterization. Appl Surf Sci 253:204–208